CHEMISTRY
A EUROPEAN JOURNAL

ChemPubSoc
Europe

DOI: 10.1002/chem.201302564

Chiral Photoresponsive Tetrathiazoles That Provide Snapshots of Folding States

Takuya Nakashima,* Kyohei Yamamoto, Yuka Kimura, and Tsuyoshi Kawai*[a]

Abstract: Herein, we designed chiral photoresponsive tetra(2-phenylthiazole)s, which induce a diastereoselective 6π-electrocyclization reaction in a helically folded structure to freeze the conformational interconversions. The folding conformation with one helical turn of tetra(2-phenylthiazole)s was supported by multiple intramolecular noncovalent interactions including vicinal S···N interheteroatom interactions and CH–π and π–π stacking interactions between nonadjacent units, as found in X-ray crystal structures as well as quantum chemical calculations. The introduction of a chiral group at both ends of tetra(2-phenylthiazole) dictates the preferential folding into a one-handed helix conformation by the simultaneous operation of S···O and multiple CH–π interactions that involve the chiral end groups. Since the tetra(2-phenylthiazole)s possess two equivalent photoreactive 6π-electron systems and the folded conformation is suitable for photoinduced electrocyclization reaction, they undergo a photocyclization reaction in a stereoselective manner to memorize the chirality of the helix in a resulting diastereomeric closed form.

Keywords: chirality · foldamers · helical structures · photochromism · supramolecular chemistry

Introduction

Foldamers have emerged as artificial oligomers that fold into well-defined secondary structures in solution, thereby mimicking biopolymers.[1] Of particular interest are the stimuli-responsive chiral helices[1–5] with respect to biomimetics since the dynamic conformational processes of proteins correlate with biological functions in natural systems. Meanwhile, light is one of the promising external inputs for various practical applications, whereby one can control the physicochemical properties of active materials with precise spatiotemporal control in a remote and noninvasive manner.[6] In this context, helical architectures that contain azobenzene units in a main framework have been developed.[7–10] The *E*–*Z* photoisomerization of the azobenzene unit serves to denature the helical structure in a dynamic manner,[7,8] which was also integrated with guest-recognition capability.[9,10] Whereas photochromes that show 6π-electrocyclization reaction such as diarylethenes[11] have been incorporated into helicenes with a rigid geometry,[12,13] chiral helical structures with the photoresponsive 6π system have never been demonstrated. The 6π-electrocyclization reaction proceeds in a quite different way from that of azobenzene with respect to the change in geometry and electronic state, which would expand the response behaviors of photoresponsive foldamers.

Recently, we have proposed an α,β-linked triheteroarylene motif called a "terarylene," which endows photochromic capability based on the 6π-electrocyclization reaction (Scheme 1).[14–16] Since the photoinduced 6π-electrocylization reaction takes place within a few picoseconds,[11] the reaction efficiency is directly dependent on the geometry around the 6π system at the ground state. Compared to conventional diarylethenes,[11] terarylenes offer better accessibility to the control of molecular folding in terms of the design of intra- and intermolecular interactions through the combination of various heteroaromatics. Despite the presence of the rotatable single bonds in the 6π system, well-designed terarylenes were able to stabilize a folded photoreactive conformation with C_2 symmetry around the 6π system in solution and achieved highly efficient photocyclization reactivity with the topmost quantum yield.[15–17] Furthermore, the photoreaction takes place in a stereospecific manner according to the Woodward–Hoffmann rule, and the conformational information of a precursor is directly recorded as the stereostructure of a photoproduct. Terarylenes with a chirally controlled geometry exhibited a photoreaction not only with high efficiency but with high stereoselectivity, which also of-

[a] Dr. T. Nakashima, K. Yamamoto, Y. Kimura, Prof. T. Kawai
Graduate School of Materials Science
Nara Institute of Science and Technology, NAIST
8916-5 Takayama, Ikoma, Nara 630-0192 (Japan)
Fax: (+81) 743-72-6179
E-mail: ntaku@ms.naist.jp
tkawai@ms.naist.jp

Supporting information for this article is available on the WWW under http://dx.doi.org/10.1002/chem.201302564.

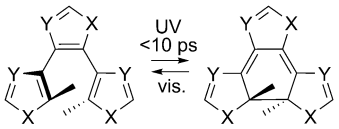

Scheme 1. Reversible photoinduced 6π-electrocyclization reaction of terarylene.

fered an advantage over diastereoselective photoreactions of diarylethenes.[18]

We envisage that further extension of terarylenes to oligoarylenes would give a stable helical structure with more than one helical turn by the addition of π–π-stacking interactions between an aryl unit and the next unit but two. α,β-Connected oligoheteroarylenes could impart photoreactivity in a main helical framework by the use of conjugated three double bonds in a *cis–cisoid* backbone. Thus, the extension of terarylenes is in line with the design of photoresponsive foldamers. In this study, we describe tetrathiazoles as a minimum building unit of a chiral photoresponsive helical motif and a prototype of a photoresponsive foldamer with 6π systems. Enantiomers of (*R*,*R*)-**1** and (*S*,*S*)-**1** (Scheme 2) were designed on the basis of tetra(2-phenylthiazole) (**2**), a single unit-extension of the terthiazole,[14a,19] the photochromic performance of which has been recently reported by Yu and co-workers.[20]

Scheme 2 depicts interconversion between representative conformers followed by a stereoselective photoreaction from the helically folded state. Steric repulsion between nonadjacent 2-phenylthiazolyl units destabilizes the all-*trans* conformer with a planar conformation and the rotation about two single bonds with 4,5-connection is expected to be harnessed by adjacent S···N interactions as demonstrated with several terarylenes.[15a,16] Since the steric repulsion still remains in the *cis–trans–cis* form with a planar structure, the central single bond with a [4′,4″]-connection rotates to adopt an all-*cis* conformation. CH–π interactions between the end alkyl substituents (R) and the thiazole ring in the next unit but one, and the π–π interaction between both the end 2-phenylthiazole units are expected to hold the all-*cis* conformer with one helical turn. The quantum chemical calculation indeed suggested that the helix conformation was the most stable among these conformers (Figure S1 in the Supporting Information). The introduction of a chiral group at both end units could dictate the preferential folding into a one-handed helix as reported in several papers by stabilizing a specific enantiomer and increasing the energy barrier of helix inversion.[21,22] The tetra(2-phenylthiazole)s possess two equivalent 6π systems,[20] and the folded conformation is suitable for a photoinduced electrocyclization reaction. Photoirradiation immediately freezes the interconversion of conformers to form a closed-ring isomer, which gives a sort of snapshot of the folding status of the photoprecursor; a right-handed helix (*P* helix) gives an *R*,*S* stereoisomer, whereas a left-handed helix (*M* helix) forms an *S*,*R* stereoisomer (Scheme 2).

A number of asymmetric reactions including diastereoselective[12,13,23] and enantioselective[24] electrocyclizations have been reported for diarylethenes in solutions, crystals, and supramolecular assemblies. These diarylethenes often tether chiral side units or adopt helicene structures to induce a chiral structure in the backbone, mainly by repulsive intramolecular interactions. The stereoselective photochromic reaction inspired by the foldamer design is demonstrated for the first time.

Results and Discussion

X-ray crystal structures and quantum chemical calculations: Recrystallization from the mixture of acetonitrile and chloroform (95:5 v/v) successfully gave single crystals of (*R*,*R*)-**1** and (*S*,*S*)-**1**. The crystallographic data for (*R*,*R*)-**1** and (*S*,*S*)-**1** together with reference compound **2** are summarized in Table 1. Each enantiomer possessed a one-handed helix with the all-*cis* conformation in the crystal as we expected in Scheme 2. The space group was $P2_12_12_1$ for both the crystals, which is typical for a chiral crystal. Compound (*R*,*R*)-**1** formed a right-handed *P* helix, whereas (*S*,*S*)-**1** adopted a left-handed *M* one with a stereostructure almost perfectly identical to the mirror image of (*R*,*R*)-**1** (Figure 1). A multitude of intra- and inter-unit noncovalent interactions were found in the crystal structure. Each 2-phenylthiazole unit formed an almost planar structure with the torsion angle below 10° supported by the CH···S and CH···N weak hydrogen-bonding interactions.[14–16,25] Compound (*R*,*R*)-**1** built a *P* helix by twisting the planar 2-phenylthiazole units in a clockwise fashion with angles of 55.18, 42.88, and 55.98° for ϕ_{A-B}, ϕ_{B-C}, and ϕ_{C-D}, respectively (Figure 1). The non-orthogonal dihedral angles for ϕ_{A-B} and ϕ_{C-D} were supported by inter-unit S–N interactions[15a,16,26] with the atomic distances of 3.306 and 3.239 Å for N(**A**)–S(**B**) and S(**C**)–N(**D**), respectively, which are shorter than the sum of van der Waals radii of S (1.8 Å) and N

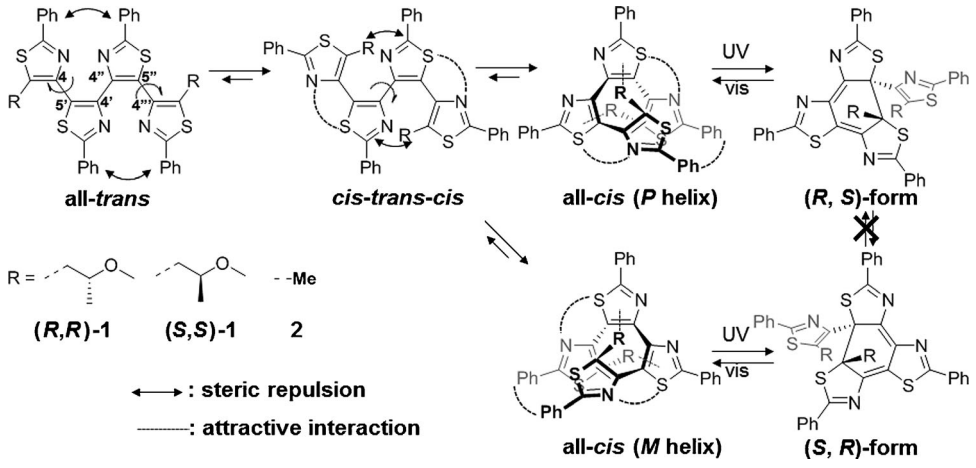

Scheme 2. Interconversion of conformers followed by reversible photochemical reactions of tetra(2-phenylthiazole)s (*R*,*R*)-**1**, (*S*,*S*)-**1**, and **2**.

Table 1. Crystallographic parameters and refinement details for (*R*,*R*)-**1**, (*S*,*S*)-**1**, and **2**.

	(*R*,*R*)-**1**	(*S*,*S*)-**1**	**2**
formula	$C_{44}H_{38}N_4O_2S_4$	$C_{44}H_{38}N_4O_2S_4$	$C_{38}H_{26}N_4S_4$
M_r	783.05	783.05	666.89
crystal system	orthorhombic	orthorhombic	monoclinic
space group	$P2_12_12_1$	$P2_12_12_1$	$P2_1/n$
a [Å]	7.8578(2)	7.8449(2)	11.9748(3)
b [Å]	22.0339(4)	22.0277(4)	13.6322(3)
c [Å]	22.3295(4)	22.3413(4)	19.9841(4)
$\alpha=\gamma$ [°]	90.0000	90.0000	90.0000
β [°]	90.0000	90.0000	96.0856(7)
V [Å^3]	3866.1(2)	3860.7(2)	3243.9(1)
Z	4	4	4
ρ [g cm^{-3}]	1.345	1.347	1.365
T [K]	123	123	123
reflns. measured	67069	66544	31760
reflns. unique	8841	8824	7432
R_1 [$I>2\sigma(I)$]	0.0296	0.0309	0.0346
wR_2 (all data)	0.0765	0.0746	0.0880

(1.55 Å). Despite the electrostatic repulsion between lone pairs of nitrogen atoms,[16] close contact of N(**B**)···N(**C**) was observed (2.891 Å). The parallel orientation of planar units **A** and **D** with the distance of 3.45 Å indicated the slipped π–π-stacking interaction between these units. In addition, multiple CH–π interactions between the chiral end group and the next unit but one (Figure 1c) could force a decrease in the torsion angle between units **B** and **C**, thereby resulting in the short atomic distance of N(**B**)···N(**C**). These intra- and inter-unit noncovalent interactions mentioned above guided the molecule to fold into compact structures with one helical turn.

The chiral end groups apparently played a crucial role in the induction of one-handed helicity since the reference compound **2** gave a racemic crystal ($P2_1/n$) that contained both-handed helices in a unit cell (Figure S4 in the Supporting Information). Interestingly, the mode of the CH–π interactions between the chiral end group and the thiazole ring in the next unit but one was most likely to determine the preferential sense of helix. Figure 1c depicts the part of the crystal structure of (*R*,*R*)-**1** around the chiral end group. The positions of hydrogen atoms were estimated theoretically. The close contact between S and O in the same unit was observed with the distance below 3.1 Å, thus indicating the S···O inter-heteroatom interactions[27] in both end units (**A** and **D**). Trapping of the ether oxygen atom in the chiral end group by thiazolyl–sulfur directed methylene, methine, and methyl protons toward the π plane of the thiazole ring in the next unit but one (broken lines in Figure 1c). The distances between these protons and the π plane were estimated to be in the range of 2.5–3.1 Å (Table S1 in the Supporting Information), which corresponds to the effective range for CH–π interactions.[28]

To confirm the difference in the noncovalent interactions on the chiral end group between *P* and *M* helices with the identical chiral end group, we calculated the optimized geometries of *P* and *M* helices of (*R*,*R*)-**1** by the DFT method using Gaussian 09.[29] For the calculation, a DFT functional ωB97XD[30] with a 6-31G(d) basis set was employed. Enantiomeric structures picked out from the identical unit cell of crystal **2** were used as initial structures after the substitution of a methyl end group with an (*R*)-2-methoxypropyl group to form both the *P* and *M* helices of (*R*,*R*)-**1**. The optimized structure starting from the *P*-helical (*R*,*R*)-**1** showed good agreement with the crystal structure of (*R*,*R*)-**1** (Figures S5 and S7 and Table S3 in the Supporting Information). The noncovalent interactions including π–π stacking between both the end units and S–O and CH–π interactions on the chiral end groups were also well reproduced in the optimized structure of *P*-helical (*R*,*R*)-**1** (Figure S8 in the Supporting Information). However, the simultaneous attainment of S···O and multiple CH–π interactions was found to be impossible in the *M*-helical (*R*,*R*)-**1**, which resulted in the higher energy of the *M* helix of (*R*,*R*)-**1** than the *P* helix of (*R*,*R*)-**1** by 8.7 kcal mol^{-1}. The DFT calculation also suggested that the *P*-helix conformation was the most stable geometry among various conformers of (*R*,*R*)-**1**, and the helix inversion needs to go through several conformers with higher energy than the *P* helix by 15.8 kcal mol^{-1} at the most (Fig-

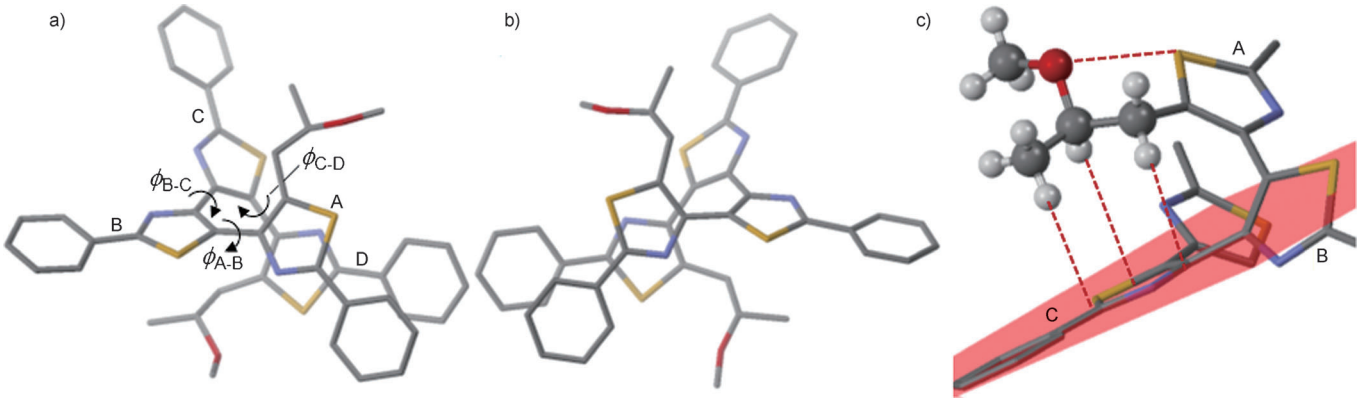

Figure 1. Crystal structures of a) (*R*,*R*)-**1** and b) (*S*,*S*)-**1**. Hydrogen atoms are omitted for clarity. c) Part of the crystal structure of (*R*,*R*)-**1** showing the intramolecular interactions (red broken lines) involving the chiral end group. The red plane includes the π-conjugated plane of the inlying 2-phenylthiazole unit (unit **C**).

ure S7 in the Supporting Information), which is much larger than the thermal energy at room temperature (0.6 kcal mol^{-1}). Thus, the DFT calculations thoroughly supported the induction of chirality in the helical handedness by the chiral end group to stabilize the helical conformation with a specific handedness and increase the energy barrier of helix inversion. It should also be noted that the even less stable *M* helix of (*R*,*R*)-**1** could be categorized as a photoreactive structure with close distances between the photoreactive carbon atoms shorter than 0.4 nm (0.346 and 0.345 nm).[31]

Circular dichroism (CD) and photochemical reaction study: We studied the chiral induction in (*R*,*R*)-**1** and (*S*,*S*)-**1** on the basis of CD spectra as demonstrated in several reports.[1–3,21,22] Compounds (*R*,*R*)-**1** and (*S*,*S*)-**1** exhibited symmetrical mirror images of their CD profiles with bisignate Cotton effects in the region of π–π-transition absorption (Figure 2a, b). Since the chiral end group itself has no π-con-

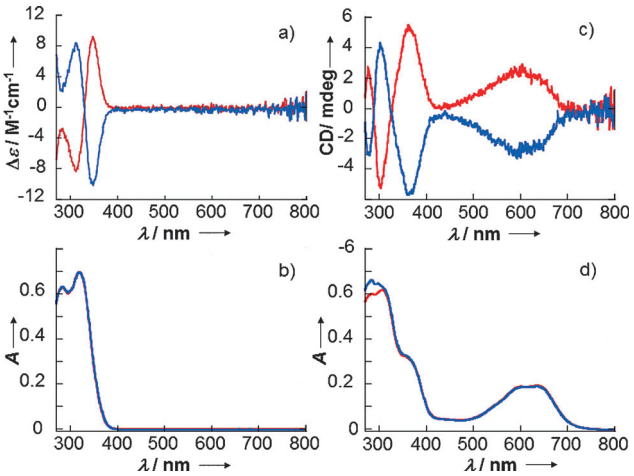

Figure 2. a, c) CD and b, d) UV/Vis spectra of (*R*,*R*)-**1** (red traces) and (*S*,*S*)-**1** (blue traces) in acetonitrile ($c = 1.5 \times 10^{-5}$ M) before (a and b) and after UV ($\lambda = 365$ nm) irradiation to achieve the photostationary state (c and d) at 298 K.

jugation system that is responsible for the absorption above 250 nm, the observed CD spectra suggested the induced chirality in the π system of the tetra(2-phenylthiazole) framework. Neither clear absorption nor a CD band was observed in the visible region before UV irradiation. According to the X-ray crystal and quantum chemical calculation studies, (*R*,*R*)-**1** and (*S*,*S*)-**1** were expected to form *P* and *M* helices, respectively. Each Cotton effect sign was positive for (*R*,*R*)-**1** and negative for (*S*,*S*)-**1**, which clearly indicated the helical arrangement or distortion of chromophores in clockwise and anticlockwise fashions, respectively. The CD spectral features were in accordance with the simulated CD profiles based on the calculated structures of the *P* helix of (*R*,*R*)-**1** and the *M* helix of (*S*,*S*)-**1** (Figure S6 in the Supporting Information). Thus the CD study clearly supported the chiral induction of helix handedness in solution.

Tetra(2-phenylthiazole)s possess two equivalent photoreactive 6π systems for the pericyclization reaction in a helically folded structure (Scheme 2). Irradiation of (*R*,*R*)-**1** and (*S*,*S*)-**1** solutions with UV light ($\lambda = 365$ nm) gave rise to the progression of a new absorption band at around 600 nm owing to the formation of pericyclized photoproducts (Figure 2d).[14,20] Meanwhile, a drastic change occurred in the CD spectra, in which broad CD signals that corresponded to the visible absorption band of photoproducts emerged after UV irradiation (Figure 2c). This CD response is characteristic of a chiral 6π system, which also demonstrated the difference to azobenzene-based chiral foldamers.[7,8] The preferential formation of *R*,*S*- and *S*,*R*-type photoisomers (Scheme 2) from (*R*,*R*)-**1** and (*S*,*S*)-**1**, respectively, were suggested, and the CD signs in the visible region were in good agreement with those simulated on the basis of time-dependent (TD)-DFT calculations (Figure S10 in the Supporting Information).[32] As demonstrated above, the photoirradiation to the helical tetrathiazoles successfully transferred and memorized their chiral information in the cyclized photoisomers. One might consider here whether the observed CD spectra are the results of the uneven existing ratios of *P* and *M* helices or *R*,*S*- and *S*,*R*-type photoproducts. To make this point clearer, we evaluated the conformational change of chiral helices in solution by means of temperature-dependent ^{1}H NMR spectroscopy, CD, and photoreaction studies.

Conformational change of tetrathiazoles studied by temperature-dependent CD and ^{1}H NMR spectroscopy: Figure 3 shows the temperature-dependent CD spectra of (*S*,*S*)-**1** in CH_2Cl_2 from 213 to 293 K. The CD peaks became prominent with a decrease in temperature. The CD intensity at the first Cotton band (350 nm) almost doubled from 293 to 213 K. This observation suggests the stabilization of the *M* helix of (*S*,*S*)-**1** at low temperature, thus leading to the in-

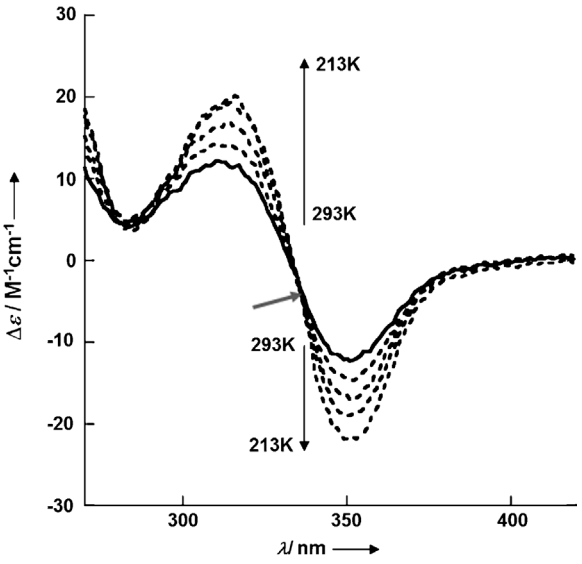

Figure 3. Temperature-dependent CD spectra of (*S*,*S*)-**1** in CH_2Cl_2. Each trace was measured at 293, 273, 253, 233, and 213 K.

crease in the population of *M* helices or the tightening of helix conformation to make it more CD-active. The helix inversion between *P* and *M* helices might fail to account for this CD spectral change since the apparent isointensity point (indicated by a gray arrow) at 338 nm was found below the baseline. If the CD change was based on the equilibrium that involves the helix inversion between *P* and *M* helices with mirror-symmetrical CD profiles, the isointensity point should be found as a zero value.

Figure 4 shows temperature-dependent ^{1}H NMR spectra of (*S*,*S*)-**1** in CD_2Cl_2. All peaks were reasonably assigned as depicted in Figure 4. In particular, the peak assignment for

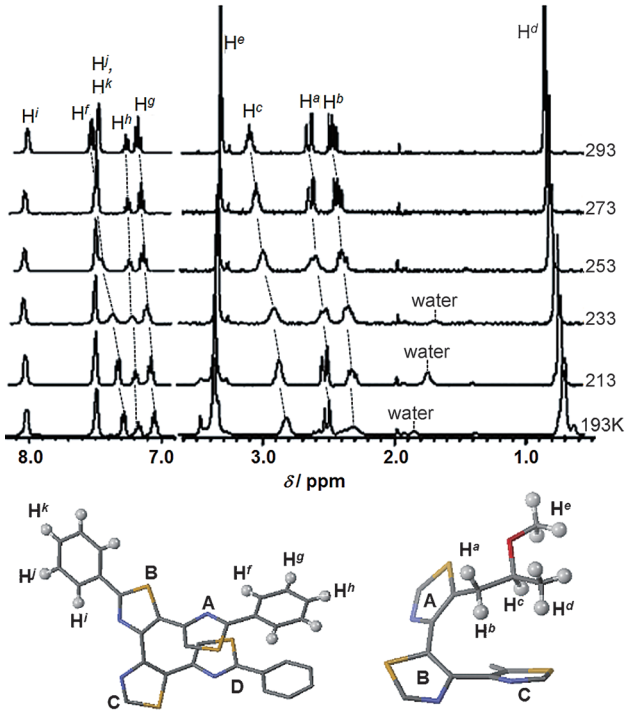

Figure 4. Temperature-dependent ^{1}H NMR spectra of (*S*,*S*)-**1** in CD_2Cl_2. The parts of the chemical structure of (*S*,*S*)-**1** are also shown for the peak assignment.

the protons on phenyl groups was on the basis of differential nuclear Overhauser effect (1D NOE) measurements. A peak that emerged at $\delta = 1.7$ ppm, which showed a downfield shift below 233 K, was due to the dew condensation water when the sample tube was chilled at low temperature. In the aliphatic region, almost all peaks except for methoxy protons (H^e) exhibited upfield shifting to varying degrees upon decreasing the temperature. The observed upfield shift for H^a–H^d clearly indicated the enhancement of CH–π interactions between these protons and thiazole ring in the next unit but one (unit C in Figure 4). The upfield shift was the most prominent for the methine proton (H^c) directly attached to the chiral carbon, and its chemical shift changed from $\delta = 3.10$ ppm at 293 K to $\delta = 2.83$ ppm at 193 K. When proton H^c approaches the face of the thiazole ring in unit C, the methylene protons (H^a and H^b) move away from the π surface of unit C to avoid the *gauche* conformation, thereby resulting in lower upfield shifting ($\Delta\delta = -0.11$ ppm from 293 to 193 K). In a similar manner, when proton H^c comes close to the thiazole in unit C, the methoxy protons (H^e) could be affected by the deshielding effect of the phenyl ring in unit D to show slight downfield shifting with decreasing temperature (Figure S11 in the Supporting Information). Thus, upon decreasing temperature, the ^{1}H NMR spectral change in the aliphatic region demonstrated enhanced interaction between the end groups and the non-adjacent π units.

Given the fact that all the phenyl groups were under a similar local electronic environment, the number of ^{1}H NMR spectroscopic peaks was supposed to be three at most. The five peaks observed in the aromatic region clearly indicated that there were two types of phenyl rings with different environments in a molecule, in which the inlying units (B and C) and both the end units (A and D) could be distinguished. Three peaks that showed continuous upfield shifting with decreasing temperature could be assigned to the protons (H^f, H^g, and H^h) in both the end units (A and D), which are anticipated to interact with each other by means of π–π stacking as observed in the crystal structure as well as the calculated structure. In comparison with the chemical shifts of H^i, H^j, and H^k that were unaltered with temperature change, those of H^f, H^g, and H^h, respectively, appeared upfield by $\delta = 0.5$–0.2 ppm at 293 K. These chemical shifts suggested that the π–π interaction between units A and D operated in solution even at room temperature to give a shielding effect to these phenyl protons.

1D NOE measurements at 293 and 203 K further confirmed the presence of a π–π interaction. The differential NOE spectra showed positive signals at peaks H^f and H^h when peak H^g was irradiated, and also a positive signal at peak H^g when H^h was irradiated at 293 K (Figure S12 in the Supporting Information). Meanwhile, these differential NOE peaks became negative at 203 K. This change from positive to negative in the differential NOE signals with decreasing temperature was clear evidence that the intra-unit correlations between vicinal protons, which are also active for ^{1}H,^{1}H COSY (homonuclear proton–proton correlation), were not responsible for these NOE signals. Moreover, it was a typical indication of the increase in the molecular correlation time owing to the stabilization of a specific molecular conformation and the slowing of molecular rotation at low temperature.[33] Therefore, ^{1}H NMR spectroscopic measurements in the aromatic region clearly supported the inter-unit spatial correlation of phenyl protons between both end units A and D by means of π–π interactions, which contributed to the stabilization of a left-handed helix of (*S*,*S*)-**1** in solution. It should be noted that no peak splitting due to the formation of minor diastereomers that corresponded to the right-handed conformation of (*S*,*S*)-**1** was observed in both aliphatic and aromatic regions in the range of temperature studied. According to the results of DFT calculations (Figure S8 in the Supporting Information), the protons in the chiral end groups were expected to have different chemical shifts between *P* and *M* helices when the inversion rate

was slow enough on the NMR spectroscopic timescale. The broadening of several peaks observed at 230 K might be attributed to the local conformational fluctuation in the *M* helix, since the peak broadening was found only for the protons associated with CH–π and π–π interactions mentioned above. Furthermore, taking the result of the temperature-dependent CD spectral change in Figure 3 into consideration, the structural fluctuation within chiral helix conformations between less and strong CD-active conformers rather than the helix inversion is most likely responsible for the conformational change. To make this point clearer, the temperature-dependent photochemical reaction was monitored by CD spectra.

Conformational change of foldamers probed by photoreaction: UV irradiation to tetra(2-phenylthiazole)s resulted in the stereoselective photochemical formation of closed-ring isomers, thus reflecting the folding status of photoprecursors in solution. Compound **2** has been reported to show an electrocyclization reaction with a quantum yield of 55% and conversion of 82%.[20] Since no chiral induction took place for **2**, unlike compound **1**, it exhibited no CD peak before and after photoirradiation. The electrocyclization reaction of **2** was expected to give two types of stereoisomers, *R*,*S* and *S*,*R* forms (Scheme 2). The relatively high thermal stability of **2** in the ring-closed isomer with a half-lifetime of the backward reaction (24 days)[20] enabled us to separate a one-enantiomer-rich solution with a chiral-phase HPLC by using hexane/ethanol (1:9) as the eluent. The separated solution gave a similar CD profile to that of the *R*,*S*-type closed form of **1** (Figure S13 in the Supporting Information). Photoirradiation with visible light induced a backward reaction to the open-form **2**.[20] After visible-light irradiation, the CD peaks disappeared even in the UV region, which showed an immediate racemization. The small methyl end groups seem insufficient to hinder the helix inversion and the transition to the excited state with a higher energy might boost the racemization.

Since the photoproducts of molecules (*R*,*R*)-**1** and (*S*,*S*)-**1** showed the spontaneous reversion to the photoprecursor states within one hour owing to the steric strain in the closed-ring forms, we could neither isolate the photoproducts nor determine the photochemical reaction quantum yield for compounds **1**. Therefore, we evaluated the conformational change of **1** by monitoring the CD intensity of the photostationary state achieved at various temperatures. Assuming that the helical inversion was responsible for the temperature-dependent CD change (Figure 3) and both the *M* and *P* helices of (*S*,*S*)-**1** were equally photoreactive, as suggested by DFT calculations, the UV irradiation at a given temperature should lead to a definite diastereomeric excess (*de*), and the relative CD intensity was supposed to increase upon decreasing temperature. Figure 5 summarizes the temperature-dependent change in the relative intensity of the CD peak for (*S*,*S*)-**1** together with that of the photostationary state achieved with UV irradiation for 1 min at given temperatures. The CD measurement for each photostationary state was conducted at room temperature. As mentioned above, the CD peak intensity of (*S*,*S*)-**1** linearly increased with decreasing temperature, and the relative intensity reached 1.77 at 213 K (see also Figure 3). The UV irradiation for 1 min gave an identical photostationary state, which was monitored by the output voltage of the photomultiplier for the DC component in the spectropolarimeter. Since the reactivity of the cycloreversion reaction was almost negligible relative to the cyclization reactivity,[20] the conversion ratio at the photostationary state was independent of temperature. Interestingly, the CD peak intensity that corresponded to the photoproduct remained almost unchanged relative to the temperature at which the photoirradiation was performed (Figure 5 and Figure S14 in the Supporting Information). This result clearly indicated that the *de* of the photoproduct was identical and the helix inversion of (*S*,*S*)-**1** did not take place in this temperature range. The chiral-phase HPLC measurement for (*S*,*S*)-**1** after UV irradiation gave only one peak for the closed-ring isomer, and no evidence of the formation of minor diastereomers was observed.

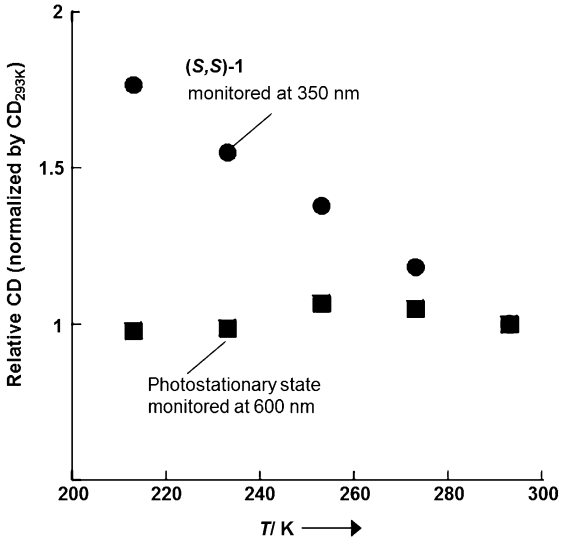

Figure 5. Plots of the relative CD peak intensity normalized by CD intensity at 293 K (CD_{293K}) for (*S*,*S*)-**1** (circles, CD monitored at 350 nm) and after 1 min UV irradiation at given temperatures (squares, CD monitored at 600 nm).

Judging from the results of our various temperature-dependent studies and DFT calculations (Figure S7 in the Supporting Information) performed, Scheme 3 could be proposed as a conclusive conformational behavior of (*S*,*S*)-**1**, whereas achiral compound **2** is expected to follow Scheme 2. The increase in CD intensity upon decreasing temperature for (*S*,*S*)-**1** could be attributed to the biased chiral induction at low temperature, and the inversion to the *P* helix with a higher energy did not take place. The induction of one-handed helicity led to the photochemical reaction with an extremely high diastereoselectivity. The induction of chirality in foldamers has often been evaluated by employing X-ray crystallography, quantum chemical calculation, CD, and

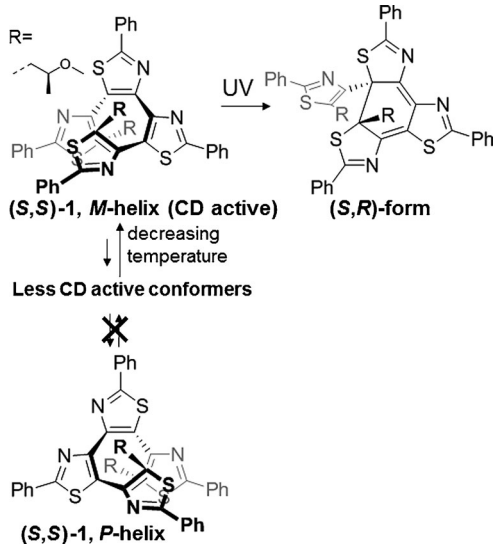

Scheme 3. Conformational change and photoreaction of (*S*,*S*)-**1**.

NMR spectroscopic measurements, as we have demonstrated in the present study.[1–5,21,22] NMR spectroscopy is sometimes found to be inadequate for monitoring helix inversion in the case that the diastereomers give identical NMR spectroscopic profiles or the rate of interconversion is faster than the NMR spectroscopic timescale. Therefore, a combination of several methods mentioned above is often employed to discuss the chiral induction quantitatively. We have herein demonstrated the photochemical conversion that takes place quickly in a stereospecific manner as a snapshot or footprint of conformational state in foldable structures since the photoproduct basically never shows global conformational change (Scheme 2). We also proved that the present system was little affected by the thermal reversion of photoproducts by CD monitoring combined with temperature-dependent photochemical reaction.

Conclusion

We have demonstrated photoresponsive chiral helical architectures based on the foldamer design as the extension of photochromic terarylenes with high 6π-electrocyclization efficiency. The X-ray crystallography, DFT calculations, and ^{1}H NMR spectroscopic study clearly suggested that the helically folded structure was stabilized by multiple intramolecular noncovalent interactions. The introduction of chiral groups at both the end units successfully induced the one-handed helicity in the crystal as well as in solution. The conformational change in solution was investigated by means of various temperature-dependent measurements, from which we concluded that no helical inversion took place. The photochemical 6π-cyclization reaction that proceeded in a stereospecific manner was proposed as a methodology for taking snapshots of folding structures as a diastereomeric photoproduct with a covalently bridged structure. The further extension of the oligoheteroarylene structure would lead to a family of photoresponsive foldamers, the secondary structures of which are controlled in a quick and dynamic manner. The chiral photoresponsive foldamers could find applications including as a chiral dopant for cholesteric liquid crystals[34,35] as well as a ligand[36] of a chiral metal complex to change its chiroptical properties. The controllability of the thermal cycloreversion reaction constant of terarylenes over seven orders of magnitude[14a,b] would add an option of duration control for those applications over a wide range of timescales including real-time modulation of chiroptical properties.[37]

Experimental Section

General: Compounds (*R*,*R*)-**1** and (*S*,*S*)-**1** were prepared according to the reaction scheme depicted in Scheme 4. Reference compound **2** was prepared according to the reported procedure.[20] Their chemical structures were confirmed by high-resolution mass spectrometry, ^{1}H NMR spectroscopy, and elemental analysis. ^{1}H NMR spectra were recorded using a JEOL AL-300 spectrometer (300 MHz). Temperature-dependent ^{1}H NMR spectra were measured using a JEOL ECP 400 spectrometer (400 MHz). Separative HPLC was performed using a JASCO LC-2000 Plus Series. Mass spectra were measured using a mass spectrometer JEOL JMS-700. Absorption spectra in solution were studied using a JASCO V-670 spectrophotometer. UV irradiation was carried out using a Panasonic Aicure UV curing system (LED, $\lambda = 365$ nm) as the exciting light source. CD spectra were recorded using a JASCO J-725 spectropolarimeter. For temperature-dependent CD studies, the temperature of samples was controlled using a Unisoku CoolSpeK cryogenic cell holder in the range from 213 K to room temperature. X-ray crystallographic analyses were carried out using a Rigaku R-AXIS RAPID/s Imaging Plate diffractometer with $Mo_{K\alpha}$ radiation. The structures were solved by direct methods (SHELXL-97) and refined by full-matrix least-squares on

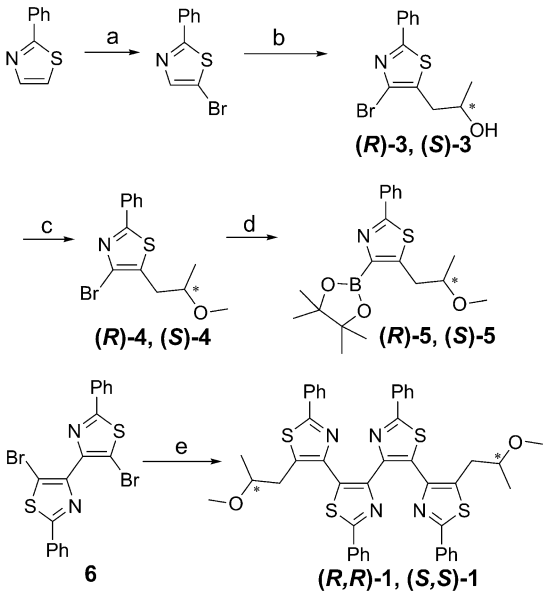

Scheme 4. Synthesis of (*R*,*R*)-**1** and (*S*,*S*)-**1**: a) NBS, $CHCl_3$, 70 °C; b) 1) LDA, THF, −78 °C, 2) (*R*)- or (*S*)-methyloxacyclopropane; c) NaH, iodomethane, THF; d) *n*BuLi, 2-isopropoxy-4,4,5,5-tetramethyl-1,3,2-dioxaborolane, THF, −78 °C; e) (*R*)- or (*S*)-**5**, $[Pd(PPh_3)_4]$, PPh_3, 2 M K_3PO_4, water/1,4-dioxane.

F^2. All non-hydrogen atoms were refined anisotropically, and all hydrogen atoms were placed using AFIX instructions. DFT calculations were performed with Gaussian 09[29] at the ωB97XD/6-31G(d) level for the open-ring forms and the B3LYP/6-31G(d) level for the closed-ring forms and TD-DFT calculations.

5-Bromo-2-phenylthiazole: *N*-Bromosuccinimide (NBS; 42 g, 0.23 mol) was added to a solution of 2-phenylthiazole (25 g, 0.16 mol) in chloroform (370 mL), and the mixture was stirred for 1 day at 70 °C. After being quenched by adding an aqueous solution of $Na_2S_2O_5$, the reaction mixture was extracted with ethyl acetate, and the combined organic layer was dried over $MgSO_4$, filtered, and concentrated. The crude product was purified with silica-gel column chromatography (ethyl acetate/hexane 1:4) to yield 5-bromo-2-phenylthiazole (15 g, 40 %) as an off-white crystalline solid. ^{1}H NMR ($CDCl_3$, 300 MHz, TMS): $\delta = 7.96$–7.92 (m, 2H), 7.48–7.43 (m, 3H), 7.22 ppm (s, 1H).

(*R*)- or (*S*)-1-(4-Bromo-2-phenylthiazol-5-yl)propan-2-ol ((*R*)-3, (*S*)-3): Lithium diisopropylamide (LDA; 29 mL, 38 mmol) in anhydrous THF (30 mL) was added portionwise to a dried four-necked flask charged with 5-bromo-2-phenylthiazole (3.0 g, 13 mmol) in anhydrous tetrahydrofuran (45 mL) under an Ar atmosphere at −78 °C. The mixture was stirred at −78 °C for 10 min, and then (*R*)-methyloxacyclopropane (1.8 mL, 30 mmol) was added to the reaction mixture and stirred for 1 day at room temperature. After the reaction was quenched by adding aqueous HCl (2 M), the reaction mixture was extracted with chloroform, and the combined organic layer was dried over $MgSO_4$, filtered, and concentrated. The crude product was purified with silica-gel column chromatography (ethyl acetate/hexane 1:4) to yield (*R*)-**3** (1.3 g, 36 %) as a yellow oil. (*S*)-**3** (0.40 g, 44 %) was also obtained from 5-bromo-2-phenylthiazole (2.0 g, 8.3 mmol) and (*R*)-methyloxacyclopropane (1.2 mL, 20 mmol). (*R*)-**3**: ^{1}H NMR ($CDCl_3$, 300 MHz, TMS): $\delta = 7.92$–7.89 (m, 2H), 7.44–7.41 (m, 3H), 3.02–2.90 (dd, $J = 15.0$, 7.2 Hz, 2H), 3.85–3.70 (m, 1H), 1.27 ppm (d, $J = 7.2$ Hz, 3H). (*S*)-**3**: ^{1}H NMR ($CDCl_3$, 300 MHz, TMS): $\delta = 7.92$–7.89 (m, 2H), 7.44–7.41 (m, 3H), 3.85–3.70 (m, 1H), 3.02–2.90 (dd, $J = 15.0$, 7.2 Hz, 2H), 1.27 ppm (d, $J = 7.2$ Hz, 3H).

(*R*)- or (*S*)-4-Bromo-5-(2-methoxypropyl)-2-phenylthiazole ((*R*)-4, (*S*)-4): NaH(60 %) (0.35 g, 8.7 mmol) and anhydrous THF (5 mL) were added to a dried four-necked flask under Ar atmosphere at 0 °C and stirred for 30 min. Compound (*R*)-**3** (1.3 g, 4.4 mmol) in anhydrous THF (5 mL) was added to the solution portionwise and stirred for 30 min. Iodomethane (0.54 mL, 8.7 mmol) was added to the mixture and stirred for another 12 h at room temperature. After being quenched by adding aqueous HCl (2 M), the reaction mixture was extracted with ethyl acetate, and the combined organic layer was dried over $MgSO_4$, filtered, and concentrated. The crude product was purified with silica-gel column chromatography using ethyl acetate/hexane (1:4) to give (*R*)-**4** (0.85 g, 62 %) as a yellow oil. Compound (*S*)-**4** was also obtained according to the same procedure as (*S*)-**3** (0.86 g, 2.9 mmol) and iodomethane (0.36 mL, 5.8 mmol) in 44 % yield (0.18 g). (*R*)-**4**: ^{1}H NMR ($CDCl_3$, 300 MHz, TMS): $\delta = 7.93$–7.90 (m, 2H), 7.43–7.41 (m, 3H), 3.63–3.52 (m, 1H), 3.39 (s, 3H), 3.01–2.95 (m, 2H), 1.24 ppm (d, $J = 7.2$ Hz, 3H). (*S*)-**4**: ^{1}H NMR ($CDCl_3$, 300 MHz, TMS): $\delta = 7.93$–7.90 (m, 2H), 7.43–7.41 (m, 3H), 3.63–3.52 (m, 1H), 3.39 (s, 3H), 3.01–2.95 (m, 2H), 1.24 ppm (d, $J = 7.2$ Hz, 3H).

(*R*)- or (*S*)-5-(2-Methoxypropyl)-2-phenyl-4-(4,4,5,5-tetramethyl-1,3,2-dioxaborolan-2-yl)thiazole ((*R*)-5, (*S*)-5): *n*BuLi (1.6 M, 2.1 mL, 3.3 mmol) was added portionwise to a dried four-necked flask charged with (*R*)-**4** (0.85 g, 2.7 mmol) in anhydrous THF (15 mL) and stirred for 30 min under an Ar atmosphere at −78 °C. 2-Isopropoxy-4,4,5,5-tetramethyl-1,3,2-dioxaborolane (0.70 mL, 3.3 mmol) was added and stirred for another 1 day at room temperature. After being quenched by adding aqueous HCl (2 M), the reaction mixture was extracted with ethyl acetate, and the combined organic layer was dried over $MgSO_4$, filtered, and concentrated to give (*R*)-**5** (0.88 g, 90 %) as a yellow oil. Compound (*S*)-**5** was prepared from (*S*)-**4** (1.0 g, 3.2 mmol) and 2-isopropoxy-4,4,5,5-tetramethyl-1,3,2-dioxaborolane (0.8 mL, 3.9 mmol) in 96 % yield. (*R*)-**5**: ^{1}H NMR ($CDCl_3$, 300 MHz, TMS): $\delta = 7.93$–7.90 (m, 2H), 7.43–7.40 (m, 3H), 3.70–3.50 (m, 1H), 3.38 (s, 3H), 3.02–2.96 (m, 2H), 1.38 (s, 12H), 1.24 ppm (d, $J = 7.2$ Hz, 3H). (*S*)-**5**: ^{1}H NMR ($CDCl_3$, 300 MHz, TMS): $\delta = 7.93$–7.90 (m, 2H), 7.43–7.40 (m, 3H), 3.70–3.50 (m, 1H), 3.38 (s, 3H), 3.02–2.96 (m, 2H), 1.38 (s, 12H), 1.24 ppm (d, $J = 7.2$ Hz, 3H).

(*R*,*R*)- or (*S*,*S*)-1: Compound (*R*)-**5** (0.20 g, 0.57 mmol), **6**[20] (90 mg, 0.28 mmol), triphenylphosphine (PPh_3, 70 mg, 0.28 mmol), 1,4-dioxane (15 mL), and aqueous K_3PO_4 (2 M, 20 mL) were added to a four-necked flask, and degassed with N_2 for 30 min. $[Pd(PPh_3)_4]$ (30 mg, 0.03 mmol) was then added to the reaction mixture and stirred for 1 day at 110 °C. After being quenched by adding aqueous HCl (2 M), the reaction mixture was extracted with ethyl acetate, and the combined organic layer was dried over $MgSO_4$, filtered, and concentrated. The crude product was purified by recrystallization (acetonitrile/chloroform 30:1) to give (*R*,*R*)-**1** (0.13 g, 60 %) as a white crystal. The enantiomer (*S*,*S*)-**1** was also prepared from (*S*)-**5** (300 mg, 0.84 mmol) and **6** (130 mg, 0.42 mmol) in 55 % yield (0.18 g). (*R*,*R*)-**1**: ^{1}H NMR ($CDCl_3$, 300 MHz, TMS): $\delta = 8.10$–8.06 (m, 4H), 7.50–7.47 (m, 10H), 7.24–7.12 (m, 6H), 3.38 (s, 1H), 3.16–3.06 (m, 2H), 2.68–2.45 (m, 4H), 0.87 ppm (d, $J = 6.0$ Hz, 6H); HRMS (ESI): *m*/*z* calcd for $C_{44}H_{38}N_4NaO_2S_4^+$ $[M+Na]^+$: 805.17753; found: 805.17769; elemental analysis calcd (%) for $C_{44}H_{38}N_4S_4$: C 67.49, H 4.89, N 7.15; found: C 67.19, H 4.65, N 7.12. (*S*,*S*)-**1**: ^{1}H NMR ($CDCl_3$, TMS, 300 MHz, TMS): $\delta = 8.10$–8.06 (m, 4H), 7.50–7.47 (m, 10H), 7.24–7.12 (m, 6H), 3.38 (s, 1H), 3.16–3.06 (m, 2H), 2.68–2.45 (m, 4H), 0.87 ppm (d, $J = 6.0$ Hz, 6H); HRMS (ESI): *m*/*z* calcd for $C_{44}H_{38}N_4NaO_2S_4^+$ $[M+Na]^+$: 805.17753; found: 805.17777; elemental analysis calcd (%) for $C_{44}H_{38}N_4S_4$: C 67.49, H 4.89, N 7.15; found: C 67.23, H 4.64, N 7.10.

Crystallographic data: CCDC-944089 ((*R*,*R*)-**1**), 944090 ((*S*,*S*)-**1**), and 944091 (**2**) contain the supplementary crystallographic data for this paper. These data can be obtained free of charge from The Cambridge Crystallographic Data Centre via www.ccdc.cam.ac.uk/data_request/cif.

Acknowledgements

We thank F. Asanoma, S. Katao, and Y. Nishikawa at NAIST for their help in the measurements and analyses with low-temperature ^{1}H NMR spectroscopy, X-ray crystallography, and HRMS, respectively. The authors also thank L. McDowell for proofreading the entire text in its original form. This research was partly supported by the Green Photonics Project at NAIST sponsored by the Ministry of Education, Culture, Sports, Science and Technology, MEXT (Japan).

[1] a) *Foldamers: Structure, Properties and Applications* (Ed.: S. Hecht, I. Huc), Wiley-VCH, Weinheim, **2007**; b) S. H. Gellman, *Acc. Chem. Res.* **1998**, *31*, 173–180; c) D. J. Hill, M. J. Mio, R. B. Prince, T. S. Hughes, J. S. Moore, *Chem. Rev.* **2001**, *101*, 3893–4011; d) I. Huc, *Eur. J. Org. Chem.* **2004**, 17–29; e) G. Guichard, I. Huc, *Chem. Commun.* **2011**, *47*, 5933–5941; f) D. W. Zhang, X. Zhao, J. L. Hou, Z. T. Li, *Chem. Rev.* **2012**, *112*, 5271–5316.

[2] a) G. Maayan, M. D. Ward, K. Kirshenbaum, *Proc. Natl. Acad. Sci. USA* **2009**, *106*, 13679–13684; b) M. S. Cubberley, B. L. Iverson, *J. Am. Chem. Soc.* **2001**, *123*, 7560–7563.

[3] C. Dolain, V. Maurizot, I. Huc, *Angew. Chem.* **2003**, *115*, 2844–2846; *Angew. Chem. Int. Ed.* **2003**, *42*, 2738–2740.

[4] a) R. B. Prince, T. Okada, J. S. Moore, *Angew. Chem.* **1999**, *111*, 245–249; *Angew. Chem. Int. Ed.* **1999**, *38*, 233–236; b) A. J. Preston, J. C. Gallucci, J. R. Parquette, *Org. Lett.* **2006**, *8*, 5885–5888; c) K. P. Divya, S. Sreejith, C. H. Suresh, A. Ajayaghosh, *Chem. Commun.* **2010**, *46*, 8392–8394.

[5] a) K. J. Chang, B. N. Kang, M. H. Lee, K. S. Jeong, *J. Am. Chem. Soc.* **2005**, *127*, 12214–12215; b) S. Ghosh, S. Ramakrishnan, *Angew. Chem.* **2005**, *117*, 5577–5583; *Angew. Chem. Int. Ed.* **2005**, *44*, 5441–5447; c) J. M. Suk, V. R. Naidu, X. Liu, M. S. Lah, K. S. Jeong, *J. Am. Chem. Soc.* **2011**, *133*, 13938–13941; d) Y. Haketa, Y. Bando, K. Takaishi, M. Uchiyama, A. Muranaka, M. Naito, H. Shibaguchi, T. Kawai, H. Maeda, *Angew. Chem. Int. Ed.* **2012**, *51*, 7967–7971.

[6] B. L. Feringa, R. A. van Delden, N. Koumura, E. M. Geertsema, *Chem. Rev.* **2000**, *100*, 1789–1816.

[7] a) A. Khan, S. Hecht, *Chem. Eur. J.* **2006**, *12*, 4764–4774; b) A. Khan, C. Kaiser, S. Hecht, *Angew. Chem.* **2006**, *118*, 1912–1915; *Angew. Chem. Int. Ed.* **2006**, *45*, 1878–1881; c) Z. Yu, S. Hecht, *Angew. Chem.* **2011**, *123*, 1678–1681; *Angew. Chem. Int. Ed.* **2011**, *50*, 1640–1643; d) Z. Yu, S. Hecht, *Chem. Eur. J.* **2012**, *18*, 10519–10524.
[8] a) C. Tie, J. C. Gallucci, J. R. Parquette, *J. Am. Chem. Soc.* **2006**, *128*, 1162–1171; b) E. D. King, P. Tao, T. T. Sanan, C. M. Hadad, J. R. Parquette, *Org. Lett.* **2008**, *10*, 1671–1674.
[9] Y. Hua, A. H. Flood, *J. Am. Chem. Soc.* **2010**, *132*, 12838–12840.
[10] Y. Wang, F. Bie, H. Jiang, *Org. Lett.* **2010**, *12*, 3630–3633.
[11] M. Irie, *Chem. Rev.* **2000**, *100*, 1685–1716.
[12] a) T. J. Wigglesworth, D. Sud, T. B. Norsten, V. S. Lekhi, N. R. Branda, *J. Am. Chem. Soc.* **2005**, *127*, 7272–7273; b) Y. Tani, T. Ubukata, Y. Yokoyama, Y. Yokoyama, *J. Org. Chem.* **2007**, *72*, 1639–1644.
[13] a) M. Takeshita, H. Jin-nouchi, *Chem. Commun.* **2010**, *46*, 3994–3995; b) H. Jin-nouchi, M. Takeshita, *Chem. Eur. J.* **2012**, *18*, 9638–9644.
[14] a) T. Nakashima, K. Atsumi, S. Kawai, T. Nakagawa, Y. Hasegawa, T. Kawai, *Eur. J. Org. Chem.* **2007**, 3212–3218; b) S. Kawai, T. Nakashima, K. Atsumi, T. Sakai, M. Harigai, Y. Imamoto, H. Kamikubo, M. Kataoka, T. Kawai, *Chem. Mater.* **2007**, *19*, 3479–3483; c) S. Kawai, T. Nakashima, Y. Kutsunugi, H. Nakagawa, H. Nakano, T. Kawai, *J. Mater. Chem.* **2009**, *19*, 3606–3611.
[15] a) S. Fukumoto, T. Nakashima, T. Kawai, *Angew. Chem.* **2011**, *123*, 1603–1606; *Angew. Chem. Int. Ed.* **2011**, *50*, 1565–1568; b) S. Fukumoto, T. Nakashima, T. Kawai, *Eur. J. Org. Chem.* **2011**, 5047–5053.
[16] T. Nakashima, R. Fujii, T. Kawai, *Chem. Eur. J.* **2011**, *17*, 10951–10957.
[17] K. Morinaka, T. Ubukata, Y. Yokoyama, *Org. Lett.* **2009**, *11*, 3890–3893.
[18] H. Ogawa, K. Takagi, T. Ubukata, A. Okamoto, N. Yonezawa, S. Delbaere, Y. Yokoyama, *Chem. Commun.* **2012**, *48*, 11838–11840.
[19] T. Nakashima, Y. Kajiki, S. Fukumoto, M. Taguchi, S. Nagao, S. Hirota, T. Kawai, *J. Am. Chem. Soc.* **2012**, *134*, 19877–19883.
[20] G. Gavrel, P. Yu, A. Leaustic, R. Guillot, R. Metivier, K. Nakatani, *Chem. Commun.* **2012**, *48*, 10111–10113.
[21] Y. Inai, K. Tagawa, A. Takasu, T. Hirabayashi, T. Oshikawa, M. Yamashita, *J. Am. Chem. Soc.* **2000**, *122*, 11731–11732.
[22] C. Dolain, H. Jiang, J. M. Leger, P. Guionneau, I. Huc, *J. Am. Chem. Soc.* **2005**, *127*, 12943–12951.
[23] a) T. Yamaguchi, K. Uchida, M. Irie, *J. Am. Chem. Soc.* **1997**, *119*, 6066–6071; b) T. Kodani, K. Matsuda, T. Yamada, S. Kobatake, M. Irie, *J. Am. Chem. Soc.* **2000**, *122*, 9631–9637; c) Y. Yokoyama, T. Shiozawa, Y. Tani, T. Ubukata, *Angew. Chem.* **2009**, *121*, 4591–4593; *Angew. Chem. Int. Ed.* **2009**, *48*, 4521–4523; d) T. Shiozawa, M. K. Hossain, T. Ubukata, Y. Yokoyama, *Chem. Commun.* **2010**, *46*, 4785–4787; e) J. J. de Jong, L. N. Lucas, R. M. Kellogg, J. H. van Esch, B. L. Feringa, *Science* **2004**, *304*, 278–281; f) T. Hirose, K. Matsuda, M. Irie, *J. Org. Chem.* **2006**, *71*, 7499–7508.
[24] a) S. Yamamoto, K. Matsuda, M. Irie, *Angew. Chem.* **2003**, *115*, 1674–1677; *Angew. Chem. Int. Ed.* **2003**, *42*, 1636–1639; b) M. Morimoto, S. Kobatake, M. Irie, *Chem. Commun.* **2008**, *44*, 335–337.
[25] R. Taylor, O. Kennard, *J. Am. Chem. Soc.* **1982**, *104*, 5063–5070.
[26] a) M. Karikomi, C. Kitamura, S. Tanaka, Y. Yamashita, *J. Am. Chem. Soc.* **1995**, *117*, 6791–6792; b) A. S. Özen, C. Atilgan, G. Sonmez, *J. Phys. Chem. C* **2007**, *111*, 16362–16371.
[27] T. Honda, H. Tajima, Y. Kaneko, M. Ban, T. Inaba, Y. Takeno, K. Okamoto, H. Aono, *Bioorg. Med. Chem. Lett.* **2008**, *18*, 2939–2943.
[28] H. Suezawa, T. Yoshida, Y. Umezawa, S. Tsuboyama, M. Nishio, *Eur. J. Inorg. Chem.* **2002**, 3148–3155.
[29] Gaussian 09, Revision B.01, M. J. Frisch, G. W. Trucks, H. B. Schlegel, G. E. Scuseria, M. A. Robb, J. R. Cheeseman, G. Scalmani, V. Barone, B. Mennucci, G. A. Petersson, H. Nakatsuji, M. Caricato, X. Li, H. P. Hratchian, A. F. Izmaylov, J. Bloino, G. Zheng, J. L. Sonnenberg, M. Hada, M. Ehara, K. Toyota, R. Fukuda, J. Hasegawa, M. Ishida, T. Nakajima, Y. Honda, O. Kitao, H. Nakai, T. Vreven, J. A. Montgomery, Jr., J. E. Peralta, F. Ogliaro, M. Bearpark, J. J. Heyd, E. Brothers, K. N. Kudin, V. N. Staroverov, R. Kobayashi, J. Normand, K. Raghavachari, A. Rendell, J. C. Burant, S. S. Iyengar, J. Tomasi, M. Cossi, N. Rega, J. M. Millam, M. Klene, J. E. Knox, J. B. Cross, V. Bakken, C. Adamo, J. Jaramillo, R. Gomperts, R. E. Stratmann, O. Yazyev, A. J. Austin, R. Cammi, C. Pomelli, J. W. Ochterski, R. L. Martin, K. Morokuma, V. G. Zakrzewski, G. A. Voth, P. Salvador, J. J. Dannenberg, S. Dapprich, A. D. Daniels, Ö. Farkas, J. B. Foresman, J. V. Ortiz, J. Cioslowski, D. J. Fox, Gaussian, Inc., Wallingford CT, **2009**.
[30] J. D. Chai, M. Head-Gordon, *Phys. Chem. Chem. Phys.* **2008**, *10*, 6615–6620.
[31] S. Kobatake, K. Uchida, E. Tsuchida, M. Irie, *Chem. Commun.* **2002**, 2804–2805.
[32] T. Hirose, J. Hasegawa, K. Matsuda, *Chem. Lett.* **2010**, *39*, 516–517.
[33] D. Neuhaus, M. P. Williamson, *The Nuclear Overhauser Effect in Structural and Conformational Analysis*, 2nd ed., Wiley-VCH, New York, **2000**.
[34] a) C. Denekamp, B. L. Feringa, *Adv. Mater.* **1998**, *10*, 1080–1082; b) T. van Leeuwen, T. C. Pijper, J. Areephong, B. L. Feringa, W. R. Browne, N. Katsonis, *J. Mater. Chem.* **2011**, *21*, 3142–3146; c) T. Yamaguchi, T. Inagawa, H. Nakazumi, S. Irie, M. Irie, *Chem. Mater.* **2000**, *12*, 869–871; d) H. Hayasaka, T. Miyashita, M. Nakayama, K. Kuwada, K. Akagi, *J. Am. Chem. Soc.* **2012**, *134*, 3758–3765; e) Y. Li, A. Urbas, Q. Li, *J. Am. Chem. Soc.* **2012**, *134*, 9573–9576; f) Y. Wang, Q. Li, *Adv. Mater.* **2012**, *24*, 1926–1945.
[35] Preliminary data for controlling the liquid-crystalline phase is shown in the Supporting Information.
[36] Y. Hasegawa, T. Nakagawa, T. Kawai, *Coord. Chem. Rev.* **2010**, *254*, 2643–2651.
[37] S. Hatano, K. Fujita, N. Tamaoki, T. Kaneko, T. Nakashima, M. Naito, T. Kawai, J. Abe, *J. Phys. Chem. Lett.* **2011**, *2*, 2680–2682.

Received: July 3, 2013
Published online: November 8, 2013

